NASA-TM-111...

NASA-92-TM
OVERRIDE
7101
P-9

Motion of the heliospheric termination shock
3. Incident interplanetary shocks

Kamcilla Naidu and Aaron Barnes

(NASA-TM-111179) MOTION OF THE HELIOSPHERIC TERMINATION SHOCK 3: INCIDENT INTERPLANETARY SHOCKS (NASA. Ames Research Center) 9 p

N96-19524

Unclas

G3/92 0101212

JOURNAL OF GEOPHYSICAL RESEARCH, VOL. 99, NO. A6, JUNE 1, 1994

JOURNAL OF GEOPHYSICAL RESEARCH, VOL. 99, NO. A6, PAGES 11,553–11,560, JUNE 1, 1994

Motion of the heliospheric termination shock
3. Incident interplanetary shocks

Kamcilla Naidu and Aaron Barnes

Theoretical Studies Branch, NASA Ames Research Center, Moffett Field, California

Abstract. In this paper the response of the heliospheric termination shock to an incident interplanetary shock is examined. This paper is an extension of a recent study by Barnes (1993), which treated the analogous problem for an incident contact discontinuity. The termination shock is treated as a strong gasdynamic shock. The postinteraction configuration consists of a moving termination shock, a postshock contact discontinuity, and either a shock or rarefaction wave propagating the disturbance signal into the downstream medium. For a decrease in dynamic pressure a rarefaction wave propagates downstream, and the new termination shock propagates inward, while for an enhancement of dynamic pressure the termination shock moves outwards and a weak outer shock propagates into the downstream medium; speeds of motion of the termination shock are typically of the order of ~100 km/s. The results are similar to those presented by Barnes (1993) indicating that the results of that paper are robust within the gasdynamic model, in the sense of being independent of the details of the initial disturbance.

1. Introduction

The equilibrium location of the heliospheric termination shock is variously estimated by various investigators [e.g., *Suess*, 1990; *Baranov*, 1990; *Holzer*, 1989; *Lee*, 1988] but may confidently be placed in the range 50–200 AU, probably with significant variation over the solar cycle [e.g., *Lazarus and Belcher*, 1988; *Lazarus and McNutt*, 1990]. The prospect of a near-term encounter of various spacecraft presently in the distant heliosphere with the shock has led to increased interest in the properties and motion of the termination shock [*Barnes*, 1991, 1993; *Smith*, 1991; *Suess*, 1993]. We expect the shock to be in constant motion [*Barnes*, 1993 (hereinafter referred to as Paper 1); *Belcher et al.*, 1993; *Suess*, 1993].

In this paper we present a simple gasdynamic model of the motion of the termination shock in response to a change in the upstream solar wind conditions. This is an extension of Paper 1, which analyzed the effect on the termination shock of an upstream jump in dynamic pressure due to a contact discontinuity (i.e., an increase (or decrease) in density with no change in the speed at the discontinuity). In that paper it was conjectured, but not demonstrated, that similar results would be obtained for initial disturbances more general than a tangential discontinuity. In this paper we explore this issue further in a model that assumes that the jump in dynamic pressure is manifested as either a forward or reverse interplanetary shock.

We construct a simple quantitative ideal gasdynamic model of the motion of the termination shock as in Paper 1. The termination shock is assumed to be a strong shock; for simplicity we take it to be initially at rest with respect to the Sun, although this assumption is not necessary. Upstream of the shock is a discontinuous increase (decrease) in dynamical pressure in the form of a forward (reverse) interplanetary shock, which eventually encounters the termination shock. The incident interplanetary shock and termination shock are both assumed to be planar and the motion is assumed to be one dimensional (in a Cartesian coordinate system) in order to make the calculation analytically tractable. While this approximation is inadequate as a global description, it is valid as a local and initial description of the interaction. In particular, it should give the correct near-term postinteraction velocity of the termination shock. Generalization to spherical geometry is desirable but will probably require numerical simulation beyond the scope of the present investigation. The analysis shows that the postinteraction configuration depends on whether the interplanetary shock is a forward or reverse shock. An encounter of a reverse interplanetary shock with the termination shock results in an inwardly moving strong shock, identified as the new termination shock, and a simple-wave rarefaction propagating downstream. In the case of an interaction between a forward shock and the termination shock the resulting configuration consists of two shocks with a contact discontinuity between them. The inner of these two shocks is an outwardly moving strong shock and is identified as the new termination shock, while the outer shock is a weak outwardly moving shock that carries the signal of the disturbance into the downstream medium. The inward and outward speeds of the new termination shock depend on the magnitude of the change in the upstream dynamic pressure but are typically of the order of 100 km/s.

The results obtained in this paper are similar to those in Paper 1. This is to be expected, as the resulting configuration after the interaction of the termination shock with incident interplanetary shocks is the same as that after an interaction with an incident contact discontinuity. Apparently, the interaction is due mainly to the arrival of a jump in dynamic pressure and depends only weakly on the details of the variation.

Paper number 94JA00581.

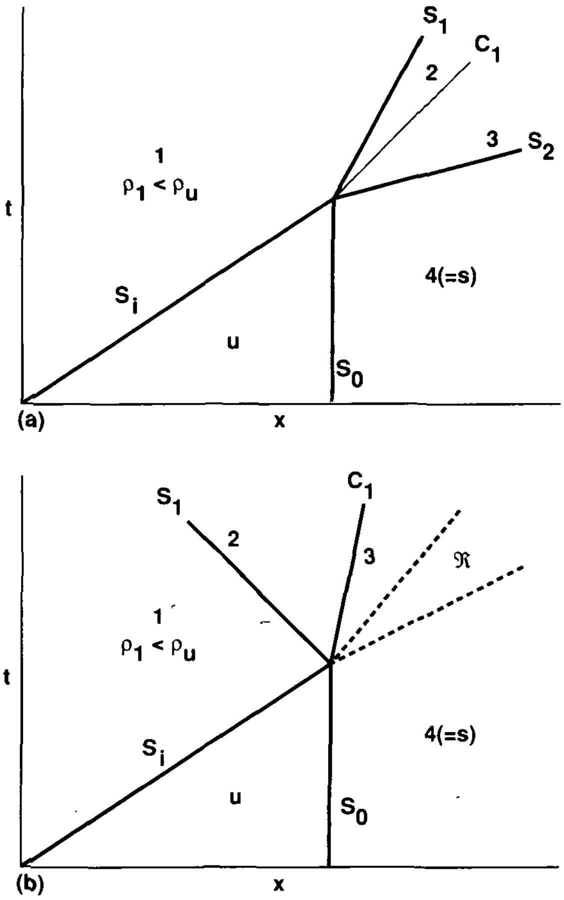

Figure 1. Schematic representation in the x-t (space-time) plane of the interaction of an upstream interplanetary shock S_i with the termination shock S_0. (a) If $\rho_1/\rho_u > 1$ after the interaction, there are two outwardly propagating shock waves S_1 and S_2 with a contact discontinuity C_1 between them. (b) If $\rho_1/\rho_u < 1$ after the interaction, there is a single inwardly propagating shock wave, a contact discontinuity C_1 and a simple-wave rarefaction $\mathfrak{R}$ propagating into the downstream.

The plan of the paper is as follows: in section 2 the assumptions of the model and details of the calculation are presented, numerical results are presented in section 3, and the conclusions are given in section 4.

2. Formal Calculation

The aim of the paper is to calculate the velocity (V_1) of the new termination shock and the velocity (V_2) of the rarefaction wave or weak second shock that propagates downstream after the interaction of an interplanetary shock with the termination shock. Consider a frame of reference Λ_0 in which the initial termination shock S_0 is static. We treat the plasma as an ideal gas whose ratio of specific heats is γ. Let ρ_u, v_u, p_u, and $c_u = (\gamma p_u/\rho_u)^{1/2}$, respectively, represent the density, velocity, pressure, and sound speed upstream of S_0, and let ρ_s, v_s, p_s, and c_s represent the corresponding quantities downstream (see Figures 1a and 1b). Let $M_{u0} = v_u/c_u$ be the Mach number upstream of S_0. We anticipate the $M_{u0} \gg 1$, although a sufficiently dense population of interstellar pickup ions in the outer heliosphere might invalidate this condition; in any case, in the formal calculations we admit all $M_{u0} > 1$. The upstream and downstream dynamical variables are related via the Rankine-Hugoniot jump conditions.

We also suppose that initially there is an interplanetary shock S_i somewhere upstream of S_0, which eventually encounters S_0. The interplanetary shock may be either a forward or reverse shock, that is, propagating either antisunward or sunward in the local plasma reference frame. Let M_{ui} be the Mach number of S_i as defined from the downstream (antisunward) side of S_i; note that M_{ui} is greater than (less than) unity if S_i is a forward (reverse) shock. Let the dynamical variables upstream of S_i be indicated by the subscript 1. Note that the density ratio ρ_u/ρ_1 is limited to the range $(\gamma - 1)/(\gamma + 1) < \rho_u/\rho_1 < (\gamma + 1)/(\gamma - 1)$. The jump conditions allow us to express M_{ui} in terms of this density ratio by

$$M_{ui}^2 = \frac{2}{(\gamma + 1)\dfrac{\rho_u}{\rho_1} - (\gamma - 1)}. \tag{1}$$

However, since M_{ui} and M_{u0} refer to the same plasma,

$$M_{ui}^2 = \left(1 - \frac{V_i}{v_u}\right)^2 M_{u0}^2, \tag{2}$$

where V_i is the velocity of S_i as measured in Λ_0. Combining these two expressions permits us to express V_i/v_u in terms of M_{u0} and the density ratio, that is,

$$\frac{V_i}{v_u} = 1 - \frac{\operatorname{sgn}\left(\dfrac{\rho_u}{\rho_1} - 1\right)}{M_{u0}} \sqrt{\frac{2}{(\gamma + 1)\dfrac{\rho_u}{\rho_1} - (\gamma - 1)}}, \tag{3}$$

where the sign of the function $\operatorname{sgn}(x) = x/|x|$ distinguishes between the forward and reverse cases for shocks S_i. Using this expression in the velocity jump condition for S_i permits us to give an explicit expression for the upstream velocity v_1,

$$\frac{v_1}{v_u} = \frac{\rho_u}{\rho_1} + \left(1 - \frac{\rho_u}{\rho_1}\right)\frac{V_i}{v_u} = 1 + \frac{\left|\dfrac{\rho_u}{\rho_1} - 1\right|}{M_{u0}} \sqrt{\frac{2}{(\gamma + 1)\dfrac{\rho_u}{\rho_1} - (\gamma - 1)}}. \tag{4}$$

Similarly, the square of the upstream sound speed c_1 is

$$\left(\frac{c_1}{v_u}\right)^2 = A\,\frac{\left(\dfrac{\rho_u}{\rho_1}\right)}{M_{u0}^2}\,\frac{\left[(\gamma + 1)\dfrac{\rho_1}{\rho_u} - (\gamma - 1)\right]}{\left[(\gamma + 1) - \dfrac{\rho_1}{\rho_u}(\gamma - 1)\right]}. \tag{5}$$

Thus, for given v_u and M_{u0} the character of the incident interplanetary shock S_i is completely determined by the density ratio ρ_u/ρ_1. When S_i encounters the initial termina-

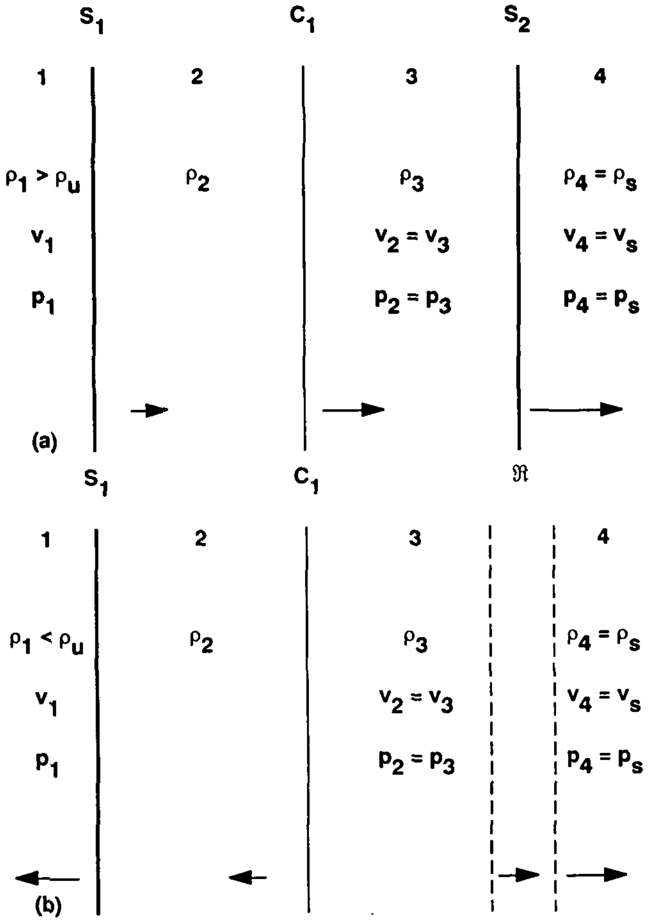

Figure 2. Schematic representation of the postinteraction geometry after an interplanetary shock has encountered the termination shock. S_1 is the postinteraction termination shock and C_1 is a contact discontinuity. (a) If $\rho_1/\rho_u > 1$, the transition between regions 3 and 4 is through a weak shock wave S_2. (b) If $\rho_1/\rho_u < 1$, the transition is through a rarefraction simple wave $\mathfrak{R}$.

tion shock S_0, the following configuration emerges as shown in Figure 2. There will be a new termination shock S_1 that will be in motion in the reference frame Λ_0. Downstream of S_1 (region 2 in Figure 2) there will be a region of shocked plasma (characterized by dynamical variables ρ_2, etc.) bounded by a contact discontinuity C_1 on the downstream side. Downstream of this discontinuity (region 3 in Figure 2) will be a region of material, originally shocked by S_0, which has responded to the disturbance created by the collision of S_0 and S_i. The signal of this disturbance will be carried to the distant downstream region either by a second shock S_2 (if S_i was a forward shock) or through a rarefaction simple wave $\mathfrak{R}$ (if S_i was a reverse shock). The far downstream region (region 4), which the disturbance signal has not yet reached, is characterized by $\rho_4 = \rho_s$, $v_4 = v_s$, $p_4 = p_s$, and $c_4 \approx c_s$.

The detailed calculation of the response closely parallels the analogous discussion of Paper 1. It is convenient to perform the analysis in the reference frame Λ_1 in which the velocity in the far downstream plasma vanishes. The velocity in this frame is denoted by u, where

$$u = v - v_4 \tag{6}$$

and $v_4 = v_s$ is the velocity of the far downstream plasma as measured in the frame Λ_0 in which the initial termination shock S_0 is static.

The far downstream gas is characterized by the following equations, derived from the jump conditions:

$$u_4 = 0$$

$$\rho_4 = \frac{(\gamma+1)M_{u0}^2}{(\gamma-1)M_{u0}^2+2}\rho_u \tag{7}$$

$$p_4 = \frac{\rho_u v_u^2}{\gamma}\frac{[2\gamma M_{u0}^2-(\gamma-1)]}{(\gamma+1)M_{u0}^2}.$$

The far downstream sound speed is given by

$$c_4 = \sqrt{\frac{\gamma p_4}{\rho_4}} = A v_u \tag{8}$$

where

$$A = \frac{1}{(\gamma+1)M_{u0}^2}\sqrt{[2\gamma M_{u0}^2-(\gamma-1)][(\gamma-1)M_{u0}^2+2]}. \tag{9}$$

The density and pressure jump conditions across the new termination shock S_1 are given by the standard jump conditions and are analogous to (17) and (18) in Paper I but with all the terms retained since we consider all $M_{11} > 0$, where M_{11} is the Mach number of region 1 with respect to S_1, and is given by

$$M_{11}^2 = \frac{(u_1 - U_1)^2}{c_1^2} \tag{10}$$

while c_1^2 is the sound speed in region 1 and U_1 the velocity of S_1 measured in the frame Λ_1.

Define the dimensionless parameter η by

$$\eta = \frac{p_3}{p_4} = \frac{\rho_1}{\rho_u}\frac{1}{v_u^2}\frac{M_{u0}^2}{2\gamma M_{u0}^2-(\gamma-1)} \cdot [2\gamma(u_1-U_1)^2-(\gamma-1)c_1^2] \tag{11}$$

where we have substituted for M_{11}^2 using (10). This expression can be rearranged to yield

$$\frac{u_1-U_1}{v_u} = \sqrt{\frac{\rho_u}{\rho_1}\eta\frac{2\gamma M_{u0}^2-(\gamma-1)}{2\gamma M_{u0}^2}+\frac{(\gamma-1)}{2\gamma}\frac{c_1^2}{v_u^2}} \tag{12}$$

where the sign is determined by the fact that region 1 is unshocked, so that $u_1 > U_1$.

Combining the expression for the velocity jump condition across S_0

$$\frac{v_4}{v_u} = \frac{\gamma-1}{\gamma+1}+\frac{2}{(\gamma+1)M_{u0}^2} \tag{13}$$

with (4), we get

$$\frac{u_1}{v_u} = \frac{v_1}{v_u}-\frac{v_4}{v_u} = \frac{2}{\gamma+1}\left[1-\frac{1}{M_{u0}^2}\right] + \frac{\left|\frac{\rho_u}{\rho_1}-1\right|}{M_{u0}}\sqrt{\frac{2}{(\gamma+1)\frac{\rho_u}{\rho_1}-(\gamma-1)}}. \tag{14}$$

The velocity jump condition across S_1, which is analogous to (20) in Paper 1, provides the following equation after substituting (10) for M_{11}^2:

$$\frac{2}{\gamma+1}(u_1-U_1)^2+(u_2-u_1)(u_1-U_1)-\frac{2}{\gamma+1}c_1^2=0. \tag{15}$$

This yields the following relation:

$$\frac{u_1-U_1}{v_u}=\frac{\gamma+1}{4}\cdot\left\{\frac{u_1-u_2}{v_u}+\sqrt{\frac{(u_1-u_2)^2}{v_u^2}+\frac{16}{(\gamma+1)^2}\left(\frac{c_1}{v_u}\right)^2}\right\} \tag{16}$$

where the positive sign must be chosen because $u_1 > U_1$.

Equating the two expressions (12) and (16) for U_1/v_u results in an expression for η in terms of M_{u0}, ρ_1/ρ_u, γ, and u_2/v_u, which may be expressed as

$$\sqrt{\frac{\rho_u}{\rho_1}\eta B+C}-\frac{\gamma+1}{4}\cdot\left\{\frac{u_1-u_2}{v_u}+\sqrt{\frac{(u_1-u_2)^2}{v_u^2}+\frac{16}{(\gamma+1)^2}\left(\frac{c_1}{v_u}\right)^2}\right\}=0 \tag{17}$$

where

$$B=\frac{2\gamma M_{u0}^2-(\gamma-1)}{2\gamma M_{u0}^2}$$

$$C=\frac{\gamma-1}{2\gamma}\left(\frac{c_1}{v_u}\right)^2$$

and c_1/v_u and u_1/v_u are given by (5) and (14), respectively.

The next task is to find an expression for u_2 as a function of η; such an expression used in (17) will permit us to solve (numerically) for η, and hence complete the solution of the problem. The expression for u_2 will depend on whether S_i is a forward or reverse shock. If S_i is a reverse shock, a rarefaction simple wave $\mathfrak{R}$ propagates into the downstream gas. $\mathfrak{R}$ has the properties outlined in Paper 1, resulting in the relation

$$u_3=\frac{2}{(\gamma-1)}(c_3-c_4)<0. \tag{18}$$

The expansion in $\mathfrak{R}$ is isentropic (equation (42) in Paper 1), and substituting (8) for c_4 results in the following expression for u_2:

$$\frac{u_2}{v_u}=\frac{u_3}{v_u}=\frac{2}{(\gamma-1)}A(\eta^{(\gamma-1)/2\gamma}-1) \tag{19}$$

where the dimensionless parameter A is given by (9). We now have an equation for u_2/v_u in terms of η and the known parameters, M_{u0}, ρ_1/ρ_u and γ.

When S_i is a forward shock ($\rho_1/\rho_u > 1$), the configuration after the interaction of S_i and S_0 will consist of a new termination shock S_1, a contact discontinuity, and a second shock S_2 that propagates the changed upstream conditions to the downstream gas. Our analysis follows Paper 1, and we consider the transition between regions 3 and 4, which involves the second shock S_2. The pressure jump condition together with definition of η (equation (11)) yields an equation analogous to (23) in Paper 1, which can be rearranged to produce

$$M_{42}^2=\frac{(\gamma+1)\eta+\gamma-1}{2\gamma}, \tag{20}$$

where M_{42}^2 is the Mach number of region 4 with respect to the shock S_2. For the configuration described above to persist $u_3 < U_2$, where U_2 is the velocity of shock S_2, which means that region 3 will contain shocked gas with $M_{42}^2 > 1$ and $\eta > 1$. Since $u_4 = 0$, $M_{42}^2 = (U_2/c_4)^2$, which yields the following expression for U_2:

$$\frac{U_2}{v_u}=A\sqrt{\frac{\gamma-1}{2\gamma}}\sqrt{1+\frac{\gamma+1}{\gamma-1}\eta}. \tag{21}$$

The continuity equation across regions (3) and (4) (with $u_4 = 0$) yields $u_3 = U_2(1 - \rho_4/\rho_3)$. Hence (21) and the jump condition for the density (see (26) in Paper 1) can be combined to give the following expression for u_2:

$$\frac{u_2}{v_u}=\frac{u_3}{v_u}=A\sqrt{\frac{2}{\gamma(\gamma-1)}}\frac{\eta-1}{\sqrt{1+\dfrac{\gamma+1}{\gamma-1}\eta}}. \tag{22}$$

Equation (22) is a function of η and the known parameters M_{u0}, ρ_1/ρ_u, and γ and can be used in (17) to solve for η.

Note that allowable η must have an upper bound. Because region (1) is unshocked

$$u_2<u_1=\frac{2}{\gamma+1}\psi\left(\gamma, M_{u0}, \frac{\rho_u}{\rho_1}\right) \tag{23}$$

where

$$\psi=\left[1-\frac{1}{M_{u0}^2}\right]+\frac{\gamma+1}{2}\frac{\left|\dfrac{\rho_u}{\rho_1}-1\right|}{M_{u0}}\sqrt{\frac{2}{(\gamma+1)\dfrac{\rho_u}{\rho_1}-(\gamma-1)}}$$

The term containing η in (22) increases monotonically for all $\eta > 1$. It then follows from (22) and (23) that $\eta < \eta_*$, where

$$\eta_*=\frac{1}{2}\left[2+\frac{\gamma+1}{\gamma-1}L^2\right]\cdot\left\{1+\sqrt{1+\frac{4(L^2-1)}{\left(2+\dfrac{\gamma+1}{\gamma-1}L^2\right)^2}}\right\} \tag{24}$$

where

$$L=\frac{\sqrt{2\gamma(\gamma-1)}}{(\gamma+1)A}\psi.$$

In the limit $M_{u0}\to\infty$ we recover (29) of Paper 1.

Table 1. Numerical Results for the Encounter of an Interplanetary Shock With the Termination Shock for $M_{u0} = 100$

	$\gamma = 5/3$			$\gamma = 2$		
$\rho_1 \rho_u$	η	V_1/v_u	V_2/v_u	η	V_1/v_u	V_2/v_u
0.25	0.452680	−0.332201	0.809170	...	...	...
	(0.445058)	(−0.334253)	(0.809017)	(0.458497)	(−0.354249)	(1)
0.333, ...	0.540191	−0.262563	0.809170	0.554146	−0.279340	1.000125
	(0.532948)	(−0.264454)	(0.809017)	(0.546483)	(−0.280413)	(1)
0.50	0.685817	−0.164614	0.809170	0.697899	−0.175103	1.000125
	(0.679863)	(−0.166073)	(0.809017)	(0.691624)	(−0.176115)	(1)
0.666, ...	0.806006	−0.095670	0.809170	0.814752	−0.101713	1.000125
	(0.801768)	(−0.096655)	(0.809017)	(0.810287)	(−0.102465)	(1)
0.80	0.889668	−0.052386	0.809170	0.895155	−0.055666	1.000125
	(0.887014)	(−0.052981)	(0.809017)	(0.892352)	(−0.056144)	(1)
1.00	1	0	0.809170	1	0	1.000125
	(1)	(0)	(0.809017)	(1)	(0)	(1)
1.25	1.126380	0.053068	0.836753	1.119508	0.056021	1.029364
	(1.122608)	(0.052326)	(0.835792)	(1.115421)	(0.055364)	(1.028257)
1.50	1.237942	0.096008	0.860066	1.224203	0.101300	1.054004
	(1.229910)	(0.094495)	(0.858258)	(1.215303)	(0.099888)	(1.051812)
2.00	1.430263	0.162994	0.898291	1.404497	0.171971	1.094569
	(1.411955)	(0.159775)	(0.894584)	(1.382493)	(0.168588)	(1.089602)
3.00	1.746130	0.257042	0.956596	∞	∞	∞
	(1.693384)	(0.248693)	(0.947027)	(1.63578)	(0.261583)	(1.1435)
4.00	∞	∞	∞	...	...	...
	(1.90866)	(0.309229)	(0.984619)	(1.82564)	(0.324419)	(1.18166)

V_1/v_u is the velocity of the postinteraction termination shock S_1 and V_2/v_u is the velocity of the second shock S_2 when $\rho_1/\rho_u > 1$, or the velocity of the head of the rarefaction wave when $\rho_1/\rho_u < 1$. The results from the calculations in Paper 1 are given in parentheses for corresponding density ratios.

3. Numerical Results

Equation (17) specifies η as a function of ρ_1/ρ_u where ρ_1/ρ_u is restricted to the range $(\gamma - 1)/(\gamma + 1) < \rho_1/\rho_u < (\gamma + 1)/(\gamma - 1)$ and u_2 is given by (19) or (22) depending on whether the initial shock is a reverse or forward shock. The termination shock velocity U_1, follows from (12) or (16), with U_2 given by (21) for a forward incident shock and the speed of the rarefaction simple wave equal to c_4 for a reverse incident shock. A Galilean transformation to the frame Λ_0, fixed with respect to the Sun, gives the velocities V_1 and V_2 of the shocks S_1 and S_2 respectively. For a reverse incident shock, V_2 is the velocity of the head of the rarefaction wave $\mathfrak{R}$ and is given by $c_4 + v_4$.

In the limiting case $\eta \to 0$, which corresponds to the expansion of the gas of region 4 into a vacuum, ρ_1, ρ_2, p_2, p_3, and c_3 all vanish, and the velocity u_2 reduces to

$$\frac{u_2}{v_u} = \frac{u_3}{v_u} = -\frac{2}{\gamma - 1} A \tag{25}$$

In the strong shock limit ($M_{u0} \to \infty$) with $c_1 = 0$ the limiting velocity of the new termination shock S_1 in the frame Λ_0 is given by

$$\frac{V_1}{v_u} = \frac{U_1}{v_u} + \frac{v_4}{v_u} = -\sqrt{\frac{2\gamma}{\gamma - 1}}. \tag{26}$$

The velocity of the head of the rarefaction wave is given by $V_2 = c_4 + v_4$. Both V_1 and V_2 are functions of M_{u0}, γ and ρ_1/ρ_u. In the limit $\eta \to 1$, $V_1 = 0$ in the strong shock limit, and $V_2 = c_4 + u_4$. In the limit $\eta \to \eta_*$, $V_1/v_u = 1$ and $V_2/v_u = (3\gamma - 1)/(\gamma + 1)$ for the strong shock case.

First, we compare the results of the present calculation with those of Paper 1 (for which the incident disturbance is a contact discontinuity). In the latter case the density ratio ρ_1/ρ_u is permitted to range from 0 to ∞, whereas in the present paper the permitted range of density ratios is $(\gamma - 1)/(\gamma + 1) < \rho_1/\rho_u < (\gamma + 1)/(\gamma - 1)$. For this range of density ratios the results of the present calculation should be identical to those of Paper 1 in the limit $M_{u0} \to \infty$. This is confirmed by in Table 1, which gives results of the present calculation for $M_{u0} = 100$, and (in parentheses) the corresponding results from the calculation of Paper 1.

The results of the present calculation should differ from those of Paper 1 by a factor of the order of $1/M_{u0}$, due to the appearance of a term of this order in (14). Table 1 shows that the calculated propagation velocities agree with those of Paper 1 to within a few percent, as expected. Also, the two values γ (2 and 5/3) give qualitatively similar results (Figure 3). Once V_1 is found other velocities of interest may be calculated:

$$\frac{v_2}{v_u} = \frac{v_3}{v_u} = \frac{1}{(\gamma + 1)M_{11}^2} \cdot \left\{[(\gamma - 1)M_{11}^2 + 2]\frac{v_1}{v_u} + 2(M_{11}^2 - 1)\frac{V_1}{v_u}\right\}$$

$$\frac{c_2}{v_u} = \frac{\sqrt{[2\gamma M_{11}^2 - (\gamma - 1)][(\gamma - 1)M_{11}^2 + 2]}}{(\gamma + 1)M_{11}^2}\left(\frac{v_1}{v_u} - \frac{V_1}{v_u}\right) \tag{27}$$

$$\frac{c_3}{v_u} = A\sqrt{\frac{\eta[(\gamma + 1) + (\gamma - 1)\eta]}{(\gamma - 1) + (\gamma + 1)\eta}} \qquad \frac{\rho_1}{\rho_u} > 1$$

$$\frac{c_3}{v_u} = A\eta^{(\gamma-1)/2\gamma} \qquad \frac{\rho_1}{\rho_u} < 1$$

where

Table 2. Numerical Results for Various M_{u0} With $\gamma = 5/3$

	$M_{u0} = 30$			$M_{u0} = 10$			$M_{u0} = 1.5$		
ρ_1/ρ_u	η	V_1/v_u	V_2/v_u	η	V_1/v_u	V_2/v_u	η	V_1/v_u	V_2/v_u
0.25	0.470626	−0.327169	0.810719	0.522813	−0.310506	0.824273	0.902936	0.080399	1.398411
0.33	0.557185	−0.257951	0.810719	0.606113	−0.242864	0.824273	0.932947	0.091849	1.398411
0.50	0.699706	−0.161068	0.810719	0.739057	−0.149566	0.824273	0.968019	0.089313	1.398411
0.67	0.815841	−0.093280	0.810719	0.843337	−0.085537	0.824273	0.986073	0.068956	1.398411
0.80	0.895807	−0.050942	0.810719	0.912797	−0.046260	0.824273	0.994060	0.045014	1.398411
1.00	1	0	0.810719	1	0	0.824273	1	0	1.398411
1.25	1.135316	0.054732	0.840245	1.161627	0.059109	0.859801	1.364223	0.107939	1.509578
1.50	1.257081	0.099393	0.865603	1.314206	0.108212	0.891517	1.779623	0.202937	1.621942
2.00	1.474394	0.170135	0.908434	1.609903	0.188359	0.948852	2.847618	0.372027	1.866426
2.50	1.673846	0.226233	0.945425	1.922765	0.255320	1.004740	4.498870	0.533206	2.172024
3.00	1.877770	0.275086	0.981310	2.315656	0.318141	1.069494	7.590468	0.711242	2.624672
3.50	2.146327	0.325049	1.026040	3.029991	0.389863	1.175600	16.29955	0.967821	3.549101
3.90	2.903426	0.400567	1.140108	6.308316	0.504641	1.555725	81.53364	1.631841	7.176246
3.99	6.942233	0.514081	1.593834	31.88829	0.638652	3.131357	786.9706	3.688561	21.037996
3.999	35.30583	0.629486	3.236902	252.1864	0.820020	8.311837	7742.927	9.953374	64.734375
4.00	∞	∞	∞	∞	∞	∞	∞	∞	∞

V_1/v_u and V_2/v_u are the velocities of the postinteraction termination shock (S_1) and the second shock (S_2) if $\rho_1/\rho_u > 1$ or speed of the head of the rarefaction wave if $\rho_1 < \rho_u$, normalized to the upstream velocity v_u.

$$M_{11}^2 = \frac{\left(\frac{v_1}{v_u} - \frac{V_1}{v_u}\right)^2}{\left(\frac{c_1}{v_u}\right)^2}$$

and v_1, c_1 and η are given by (4), (5), and (11).

Let us now consider lower values of M_{u0}. At distances of ~50 AU the measured proton temperature is typically of the order of a few times 10^4K, at least at low heliographic latitude [*Gazis et al.*, 1994], and varies only slowly with heliocentric distance. No measurements of the electron temperature are available beyond ~5 AU, but if we assume that the electron temperature is comparable to the proton temperature, then M_{u0} will be in the range ~8–30 for a solar wind speed of 400 km/s. A population of interstellar pickup ions sufficiently hot and dense to amount to an appreciable fraction of the solar wind pressure would imply a lowering of this estimate. Table 2 shows results for $M_{u0} = 30$, 10, and 1.5, with $\gamma = 5/3$ (results for $\gamma = 2$ are similar and not given here). The results for $M_{u0} = 30$ and 10 are similar to each other and to the results for $M_{u0} = 100$ (Table 1). The behavior of the new termination shock and the second shock or rarefaction wave does not vary qualitatively for values of M_{u0} down to ~2.4. However, at values of M_{u0} lower than 2.4 the new termination shock may move inward or outward depending on the value of the density ratio. When M_{u0} reaches 1.6, the motion of the termination shock is outward for all permitted values of the density ratio, as shown in Table 2 for $M_{u0} = 1.5$.

For larger M_{u0} values the inward shock speeds for density ratio decreases are typically larger than the outward shock speeds for comparable density ratio increases. However, as M_{u0} decreases, these speeds approach similar values until $M_{u0} \sim 24$. Then, for density ratios near unity the outward shock speed for a density increase is larger than the inward shock speed for a corresponding density decrease. The range of ratios for this occurrence becomes larger with further decreasing M_{u0}. For $M_{u0} < 2.4$ the new termination shock S_1 can assume either inward or outward excursions depending on the density ratio decrease as shown in Figure 4. In these cases the outward shock speed for $\rho_1/\rho_u > 1$ is always greater than the outward shock speeds for a comparable decrease in density ratio. The speed of the weak outward moving shock wave is significantly faster for lower values of M_{u0}, as illustrated in Figure 4.

A singularity arises in the solutions as $\rho_1/\rho_u \rightarrow (\gamma + 1)/(\gamma - 1)$. In this limit, (3)–(5) give infinite v_1, V_i, and c_1, corresponding to an infinitely strong incident interplanetary shock S_i. However, the speed V_1 of the new termination shock increases only very slowly in this limit; for example, even for the extreme case $\rho_1/\rho_u = 3.99$, for which the far upstream solar wind velocity $v_1 = 9.3\ v_u$ (~3700 km/s) the speed of the new termination shock is only $V_1 = 0.82\ v_u$ (~330 km/s).

Altogether the results of the present calculation are qualitatively similar to the results of Paper 1, except for the extreme cases of small M_{u0} and effectively incident interplanetary shocks of near-infinite strength.

4. Conclusion

The motion of the termination shock resulting from interaction with an interplanetary shock has been studied. Our analysis shows that the postinteraction configuration depends upon whether the jump in density associated with the interplanetary shock, which is restricted to the range $(\gamma - 1)/(\gamma + 1) < \rho_1/\rho_u < (\gamma + 1)/(\gamma - 1)$, is greater or less than 1. In the case of a density increase ($\rho_1 > \rho_u$) the termination shock moves outwards, while for a decrement ($\rho_1 < \rho_u$) the resulting motion of the termination shock is inward for reasonable values of M_{u0}. For larger M_{u0} values (>24) the speed of the inward propagating shocks are slightly higher than those of the outward propagating shocks at comparable density ratios while for smaller M_{u0} (<24) the speed for the outward motion tends to be larger, particularly at density ratios close to 1. The speeds of both inward and outward propagating shocks are typically of the order of 100 km/s. Some peculiarities arise for the extreme cases of small M_{u0} and an infinitely strong incident interplanetary shock (see section 3); however, neither of these regimes is significant in practice.

These results are qualitatively similar to those in Paper 1 for physically reasonable values of M_{u0}, illustrating that the conclusions drawn from Paper 1 are robust. It should be noted, however, that in Paper 1 an infinite range of ρ_1/ρ_u is permitted, whereas in the present paper the corresponding range is limited by the jump conditions for the interplanetary shocks. The results of the present study suggest that in the gasdynamic limit a discontinuous change in pressure can be adequately described by a contact discontinuity incident on the termination shock.

In this model, various simplifications have been made. One is that the heliospheric magnetic field has been ignored. However, as shown in Paper 1, there is an isomorphism between the solutions for $\gamma = 2$ magnetohydrodynamics and $\gamma = 2$ gasdynamics, which is valid for any combination of adiabatic flows and shocks. Hence the results presented in Table 1 for $\gamma = 2$ would be the same in the MHD case if η is interpreted as P_3^*/P_4^*, where $P^* = p + B^2/4\pi$. This result is not expected to hold for $\gamma \neq 2$ or if there is a nonzero component of the magnetic field in the flow direction; however, the conclusions of the paper are not expected to be greatly modified with the inclusion of MHD effects.

A further simplification has been the neglect of the anomalous cosmic ray component, which *Jokipii and Kota* [1990] suggest could play an important part in governing the structure and behavior of the shock. As explained in Paper 1, appreciable energy would be used to accelerate the anomalous component, which would affect the jump conditions and shock structure and thickness. Analyses of the even more extreme situation in which a shock is modified by galactic cosmic rays indicate that the shock structure can be quite broad and complex [e.g., *Drury and Völk*, 1981; *Axford et al.*, 1982]. *Donohue and Zank* [1993] have recently presented a model of the termination shock that incorporates a parametric model of acceleration of the anomalous component; their results give an estimate of shock thickness (what they call the foreshock) of about 1 AU. It should be noted, however, that under the assumptions of the *Donohue and Zank* [1993] model the galactic cosmic rays dominate the structure and dynamics of the shock, so that their results do not give a clear picture of the situation as it would be if the acceleration of the anomalous component should be a large effect, while galactic cosmic rays were relatively unimportant.

Another important simplification has been the treatment of the shocks as planar, which only gives a reasonable description of the local and near-term response of the termination shock to a change in the upstream dynamic pressure. An adequate global description would require generalization of the model to at least spherical symmetry. We have also assumed that the plasma upstream of the incident shock is uniform, whereas in reality it may vary on length scales of several astronomical units. A detailed analysis of this situation would require numerical simulation. Donohue and Zank have simulated such shock pulse collisions, for which the postinteraction termination shock evolves back to its original state, for both the gas dynamic and cosmic ray dominated cases (cf. Figures 8–11 of that paper). As one would expect, the region around the postshock contact discontinuity is considerably more complicated than in the cases considered in the present paper. It is not apparent from the Donohue and Zank paper whether the interaction results in the final termination shock being in motion relative to the position of the initial termination shock, as was the case for self-canceling density discontinuities discussed in Paper 1 (cf. Figure 4 of that paper).

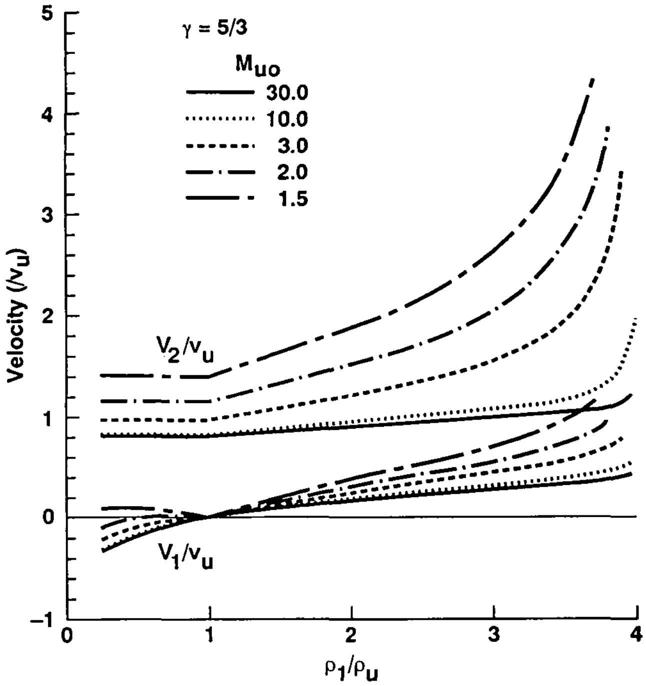

Figure 4. Plots of V_1/v_u and V_2/v_u as a function of ρ_1/ρ_u for various M_{u0} values with $\gamma = 5/3$.

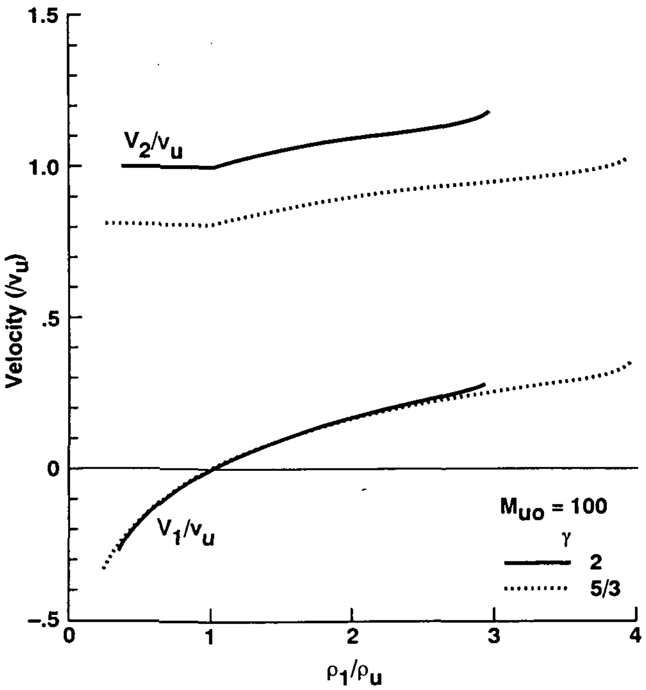

Figure 3. Plots of V_1/v_u and V_2/v_u as a function of the density ratio ρ_1/ρ_u for $\gamma = 5/3$ and $\gamma = 2$ with $M_{u0} = 100$. The velocities are in the rest frame Λ_0. V_1 is the velocity of the postinteraction termination shock S_1, and V_2 is the velocity of the shock S_2 if $\rho_1/\rho_u > 1$, or the velocity of the head of the rarefaction wave $\mathfrak{R}$ if $\rho_1/\rho_u < 1$.

Acknowledgments. This research was carried out during the tenure of one of the authors (K.N.) as a National Research Council Resident Research Associate at the Ames Research Center.

The Editor thanks G. P. Zank and M. A. Gruntman for their assistance in evaluating this paper.

References

Axford, W. I., E. Leer, and J. F. McKenzie, The structure of cosmic ray shocks, *Astron. Astrophys.*, *111*, 317–325, 1982.

Baranov, V. B., Gas dynamics of the solar wind interaction with the interstellar medium, *Space Sci. Rev.*, *52*, 89–128, 1990.

Barnes, A., J. D. Mihalov, and P. R. Gazis, Prospects for detection of the heliospheric terminal shock: ARC plasma analyzer aboard Pioneer 10, *Eos Trans. AGU*, *72*, Spring Meeting suppl., 387, 1991.

Barnes, A., Motion of the heliospheric termination shock: A gas dynamic model, *J. Geophys. Res.*, *98*, 15,137–15,146, 1993.

Belcher, J. W., A. J. Lazarus, R. L. McNutt, Jr., and G. S. Gordon Jr., Solar wind conditions in the outer heliosphere and the distance to the termination shock, *J. Geophys. Res.*, *98*, 15,177–15,183, 1993.

Courant, R., and K. O. Friedrichs, *Supersonic Flow and Shock Waves*, Interscience, New York, 1948.

Donohue, D. J., and G. P. Zank, The steady-state and dynamical structure of a cosmic-ray-modified termination shock, *J. Geophys. Res.*, *98*, 19,005–19,025, 1993.

Drury, L. O'C., and H. J. Völk, Hydromagnetic shock structure in the presence of cosmic rays, *Astrophys. J.*, *248*, 344–351, 1981.

Gazis, P. R., A. Barnes, J. D. Mihalov, and A. J. Lazarus, Solar wind velocity and temperature in the outerheliosphere, *J. Geophys. Res.*, *99*, 6561–6573, 1994.

Holzer, T. E., Interaction between the solar wind and the interstellar medium, *Ann. Rev. Astron. Astrophys.*, *27*, 199–234, 1989.

Jokipii, J. R., and J. Kota, Energy, density, and spectrum of the anomalous component, *Proc. Int. Conf. Cosmic Rays 21st*, *6*, 198, 1990.

Lararus, A. J., and J. Belcher, Large-scale structure of the distant solar wind and heliosphere, in Proceedings of the Sixth International Solar Wind Conference, edited by V. J. Pizzo, T. Holzer, and D. G. Sime, *Tech. Note NCAR/TN-306+Proc*, pp. 533–537, Natl. Cent. for Atmos. Res., Boulder, Colo., 1988.

Lararus, A. J., and R. L. McNutt, Plasma observations in the distant heliosphere: A view from Voyager, in *Physics of the Outer Heliosphere*, edited by S. Grzedzielski and D. E. Page, pp. 229–234, Pergamon, New York, 1990.

Lee, M. A., The solar wind terminal shock and the heliosphere beyond, in Proceedings of the Sixth International Solar Wind Conference, edited by V. J. Pizzo, T. Holzer, and D. G. Sime, *Tech. Note NCAR/TN-306+Proc*, pp. 635–650, Natl. Cent. for Atmos. Res., Boulder, Colo., 1988.

Smith, E. J., Capabilities of Pioneer and Voyager instrumentation to detect the termination shock and upstream phenomena, *Eos Trans. AGU*, *72*, Spring Meeting suppl., 387, 1991.

Suess, S. T., The heliopause, *Rev. Geophys.*, *28*, 97–115, 1990.

Suess, S. T., Temporal variations in the termination shock distance, *J. Geophys. Res.*, *98*, 15,147–15,155, 1993.

A. Barnes and K. Naidu, Theoretical Studies Branch, NASA Ames Research Center, Moffett Field, CA 94035-1000. (e-mail: Internet naidu@windee.span.nasa.gov; barnes@windee.arc.nasa.gov)

(Received April 22, 1993; revised January 13, 1994; accepted February 16, 1994.)